Baryon-baryon scattering in a one-boson-exchange-potential approach. I. Nucleon-nucleon scattering

M. M. Nagels,† T. A. Rijken,† and J. J. de Swart
Institute for Theoretical Physics, University of Nijmegen, Nijmegen, The Netherlands
(Received 21 April 1975)

From a combined analysis of nucleon-nucleon and hyperon-nucleon scattering with a one-boson-exchange-potential-model the *NN* results are presented. The model consists of local potentials due to exchanges of members of the pseudoscalar and vector meson nonets and the scalar meson ϵ taken as a unitary singlet. Effects of the large widths of the ϵ and ρ meson are included. The Schrödinger equation is solved in configuration space with phenomenological hard-core potentials at short distances. The coupling constants and hard-core radii are determined in a fit using the *NN* phase-shift analysis of the Livermore group up to 330 MeV laboratory kinetic energy and the low-energy parameters. The *NN* phase shifts are described well with χ^2/data = 2.4 (as good as the purely phenomenological potentials) and good values are obtained for the scattering lengths, effective ranges, and deuteron parameters.

I. INTRODUCTION

Extensive work in the past decade (for references see the reviews of Refs. 1–4) shows that the long- and medium-range nuclear forces can be described more or less satisfactorily by a sum of one-boson-exchange potentials (OBEP). However, many of these models had to use unrealistic values for the meson-nucleon coupling constants and meson masses. To get sufficient attraction one had to introduce either an uncorrelated two-pion-exchange potential (TPEP) or some scalar mesons. The advantage of the introduction of the scalar mesons is that they also give sizable spin-orbit potentials besides attractive central potentials. But to get a good fit to the *NN* data the mass of an $I=0$ scalar meson (often called σ meson) had to be unrealistically low: $m_\sigma \simeq 400$–500 MeV. No evidence for such a meson has been found in nature.[5] Recently the situation with respect to the OBEP models improved considerably.[6] One of the most important innovations has been the inclusion of effects due to the large width of the ϵ meson, thus getting rid of the fictitious σ meson with low mass.

Our program, outlined in more detail in Ref. 7, is to construct potential models which can describe simultaneously all experimentally studied baryon-baryon (BB) systems up to the pion production threshold: nucleon-nucleon and hyperon-nucleon scattering. The models in Ref. 6 were evaluated in momentum space by solving the Blanckenbecler-Sugar equation or the Lippmann-Schwinger equation. Working in momentum space has the advantage that momentum-dependent effects can be included easily. We evaluate our models in configuration space by solving the Schrödinger equation with local potentials, having the advantage that Coulomb effects can be included easily, and it permits simple parametrizations for the short-range repulsion in the form of hard or soft cores. At first we constructed an OBEP + TPEP model, called model A (Refs. 7 and 8), consisting of OBEP from the members of the pseudoscalar- and vector-meson nonets, and the Brueckner and Watson TPEP. Model A, intended primarily for a good description of the low-energy *YN* data, gave a reasonable account of the *NN* *s* waves, but failed to give a good quantitative description of the *NN* higher waves.

In our study of the pure OBEP models we insist on dealing with the mesons in an SU(3) consistent way. One reason for this is that only then can we extend our *NN* calculations also to the *YN* channels. Another, no less important, reason is that only when one uses the meson spectrum and the meson-nucleon coupling constants as realistically as possible can one expect that the determined coupling constants make any sense. For example, from the vector-meson nonet one should include in *NN* calculations the ρ, ω, and ϕ mesons, and one should use all our SU(3) knowledge about the ω-ϕ mixing and about the coupling constants. The potential due to ω and ϕ exchanges cannot be simulated sufficiently accurately in general by a potential due to some effective ω only. From the pseudoscalar-meson nonet one should include the η as well as the X^0. In many *NN* models the η or X^0 are often discarded because their contributions can be hardly separated in *NN*, and they are replaced then for convenience by some effective X^0 or η.

The OBEP models we studied so far can be divided into two classes. The long- and medium-range forces are given in all these models by the sum of the pole contributions of the members of

the pseudoscalar- and vector-meson nonets. The classes differ in the treatment of the scalar mesons. In the first class the existence of only one unitary singlet scalar meson, called ϵ, is assumed with a mass in the neighborhood of 700 MeV and a very large width. The models in the second class contain, in addition, an octet of scalar mesons. The reason for these classes is that we want to test with models in class I the assumption of the ϵ being dominantly a unitary singlet. In the fit to YN models in class II we have one more free parameter[9] [α_S, the $F/(F+D)$ ratio of the scalar nonet] and the mass or even the existence of the strange scalar meson, the κ, is very uncertain.[5] Furthermore, we want to study the effects of the octet of scalar mesons in the differences between the classes I and II. The first model in class I, called model B,[8] had the pole parameters for the ϵ: $m_\epsilon = 720$ MeV, $\Gamma_\epsilon = 400$ MeV. It gave a reasonable description of NN with $\chi^2/\text{data} = 5.9$ for the data up to 330 MeV. A better fit was obtained already in the first model in class II: model C,[9] yielding $\chi^2/\text{data} = 4.0$. In model C different pole parameters for the ϵ were used: $m_\epsilon = 670$ MeV, and $\Gamma_\epsilon = 500$ MeV. The present model D falls in class I. The main differences with model B are: (i) It contains η-X^0 mixing; (ii) the ϵ-pole parameters have been changed: $m_\epsilon = 760$ MeV and $\Gamma_\epsilon = 640$ MeV; (iii) a larger value for α_P, the $F/(F+D)$ ratio for the pseudoscalar octet, results from the analysis of the YN channels, which is the subject of paper II (see Ref. 10); (iv) the potential forms of the vector and scalar mesons have been changed slightly; and (v) there is a drastic improvement of the fit to $\chi^2/\text{data} = 2.4$ for model D. Summarizing the considered mesons, model D contains:

(i) the pseudoscalar-meson nonet, π, η, and X^0, with the singlet-octet mixing angle from the Gell-Mann–Okubo mass formula, $\theta_P = -10.4°$;

(ii) the vector-meson nonet, ρ, ϕ, and ω, with ideal mixing $\tan\theta_v = 1/\sqrt{2}$;

(iii) the scalar-meson unitary singlet ϵ.

The ϵ and ρ mesons are treated as broad mesons. Effects of the width have been taken into account by assuming for the propagator in the timelike region a Breit-Wigner–type form with proper threshold behaviour continued analytically to spacelike values of the momentum transfer.[11,12] It appears that one can describe the potential due to these broad mesons very accurately for our purpose by a sum of the potentials of two effective narrow mesons with different masses. The lower mass (≈ 510 MeV) in the two-poles approximation for the ϵ explains the traditional σ.

For very short ranges ($r \lesssim 0.5$ fm) we assume a strong repulsion in all channels, which is described phenomenologically by using hard-core potentials. It should represent many unclear short-range effects due to, e.g., exchanges of very heavy mesons (A_1, B, f, ...), coupling to negative energy states, inelastic effects, etc. A different method one uses often is the introduction of form factors for the propagators[6] or at each vertex.[13] These form factors lead in configuration space to less singular or even regular potentials near $r = 0$. The disadvantage of this approach seems to us to be that only the meson dynamics is modified so as to make the Schrödinger or Blankenbecler-Sugar equation solvable, but there is almost no independent phenomenological representation for the short-range effects. The hard-core parametrization has the virtue that it is rather independent of the considered meson dynamics.

The radii of the hard cores, x_s for $^1S_0$, x_t for $^3S_1$-$^3D_1$, x_p for $L = 1$, and $x_{L\geq 2}$ for $L \geq 2$ waves, are free parameters. In addition, the model contains 8 free meson-nucleon couplings: $g(\pi)$, $g^1(X^0)$, $g(\rho)$, $f(\rho)$, $g^1(\omega)$, $f(\omega)$, $f(\phi)$, and $g(\epsilon)$, where $g^1(X^0)$ and $g^1(\omega)$ denote the unitary singlet parts of the X^0 and ω couplings. The NN analysis happens to be unable to give a good splitting between the physical coupling constants $g(\eta)$ and $g(X^0)$. Various combinations of $g^8(\eta)$ and $g^1(X^0)$ can give the same χ^2, where $g^8(\eta)$ denotes the octet part of the physical η coupling. On the other hand, YN is very sensitive to the value of α_P, the $F/(F+D)$ ratio for the pseudoscalar octet. Therefore we determine α_P in the fit to YN,[10] leading to a particular value of $g^8(\eta)$. The NN fit then pinpoints $g^1(X^0)$. For the direct coupling of the vector mesons we keep $\alpha_V^e = 1$, thus coupling the ρ meson universally to the isospin current.[14] Via $g(\rho)$ and $\alpha_V^e = 1$ the physical coupling constants $g(\omega)$ and $g(\phi)$ are fixed simultaneously by $g^1(\omega)$. As to the derivative couplings of the vector mesons, it appears that $f(\rho)$ and $f(\omega)$ are very well determined, but the sensitivity to $f(\phi)$ is rather small. Therefore α_V^m and hence $f_{NN\phi}$ is checked in the YN analysis,[10] yielding about the same order of uncertainty as in NN.

The 12 free parameters are determined in a fit to the low-energy parameters and the χ^2 surface data of the energy-independent phase-shift analysis of the Livermore group[15] from 25–330 MeV, which yields for small deviations from their phase-shifts the proper χ^2 with respect to 1128 experimental data.

We note that the obtained $\chi^2/\text{data} = 2.4$ for pp and np is even lower than Reid's phenomenological hard-core (HC) potentials,[16] which give $\chi^2/\text{data} = 2.7$ for pp (Ref. 2). We want to point out that meson-theoretical potentials should be preferred above

purely phenomenological ones. Firstly, we have potentials acting in all waves in contrast to Reid's potentials which are only given for s, p, and d waves. Secondly, because of the big difference in number and accuracy between the pp and np data the $I=1$ phenomenological potentials will be determined very well by pp in contrast to the $I=0$ potentials, which are determined by the np data alone. In the meson-theoretical case the free parameters (coupling constants and short-range parameters) are fixed mainly by the accurate pp data, thus producing at the same time reliable $I=0$ potentials.

An important difference with model A is that beyond contributions leading to central, spin-spin, tensor, and spin-orbit potentials we consider in all later models also contributions leading to quadratic spin-orbit potentials. So we have for NN a complete set of independent potential forms[17] for $I=0, 1$, when the p-n mass difference is neglected. The quadratic spin-orbit potentials are important for the description of the p and d waves (see also the Hamada-Johnston and Yale potentials[18,19]). Omission of these potentials would introduce bias in the determination of the meson couplings.

The searched values for the meson-nucleon coupling constants are realistic. The NN phase-shifts are described very well. In particular we note that we find agreement for ϵ_1 at higher energies with the values of the phase-shift analyses, which seems to be a problem for most meson-theoretical models.[3]

The plan of the paper is as follows: In Sec. II we describe the model. The results for the coupling constants, phase shifts, s- and p-wave scattering lengths, and effective ranges and deuteron parameters are presented in Sec. III. The coupling constants are discussed in Sec. IV, where we also analyze the results for the phase shifts and low-energy parameters.

II. THE MODEL

The NN interactions are described by local potentials of the form

$$V = V_C + V_\sigma \vec{\sigma}_1 \cdot \vec{\sigma}_2 + V_T S_{12} + V_{SO} \vec{L} \cdot \vec{S} + V_Q Q_{12}. \quad (1)$$

The local functions V_i ($i = C, \sigma, T, \mathrm{SO}, Q$) can be decomposed as

$$V_i = V_i^{(0)} + \vec{\tau}_1 \cdot \vec{\tau}_2 V_i^{(1)}, \quad (2)$$

where $V_i^{(0)}$ and $V_i^{(1)}$ represent the contributions of the exchanges of the $I=0$ and $I=1$ mesons, respectively.

In the derivation of the potentials V_i from field theory the following approximations are made[20]:

(i) The dependence on the total energy is neglected.

(ii) The energy factors are expanded as

$$E = \left(\frac{\vec{q}^2}{4} + \vec{p}^2 + M^2\right)^{1/2} \simeq M + \frac{\vec{q}^2}{8M}, \quad (3)$$

where $\vec{q}$ and $\vec{p}$ denote the momentum transfer and the total momentum and M denotes the nucleon mass. In the final expressions for the potentials in momentum space, terms are kept up to first order in $\vec{q}^2/M^2$.

(iii) the contributions to the quadratic spin-orbit potentials are coming only from the Pauli spin operators in the Dirac spinors and γ matrices. Possible contributions via recoil effects are neglected, since these expressions depend on the total energy. Hence the pseudoscalar γ_5 coupling does not yield potentials of this type. In the Fourier transform to configuration space[21] we neglect all terms involving $\vec{\nabla}_r$, apart from the ones occurring in the operators $\vec{L}$, i.e., we make the approximation

$$\int \frac{d^3q}{(2\pi)^3} e^{i\vec{q}\cdot\vec{r}} [\vec{\sigma}_1 \cdot (\vec{q}\times\vec{p})][\vec{\sigma}_2 \cdot (\vec{q}\times\vec{p})] \tilde{V}(q) \simeq -\left[\left(\frac{1}{r}\frac{\partial}{\partial r}\right)^2 V(r)\right] Q_{12}. \quad (4)$$

Here $V(r)$ denotes the Fourier transform of $\tilde{V}(q)$, and

$$Q_{12} = \tfrac{1}{2}[(\vec{\sigma}_1 \cdot \vec{L})(\vec{\sigma}_2 \cdot \vec{L}) + (\vec{\sigma}_2 \cdot \vec{L})(\vec{\sigma}_1 \cdot \vec{L})]. \quad (5)$$

Below we list the field-theoretical Hamiltonian densities (suppressing isospin) and the corresponding NN potentials.

(a) Pseudoscalar-meson exchange. We have

$$H_P = i g_P \bar{\psi} \gamma_5 \psi \varphi_P \quad (6)$$

and

$$V_P = \frac{g_P^2}{4\pi} \frac{m^2}{4MM'} m[\tfrac{1}{3}(\vec{\sigma}_1 \cdot \vec{\sigma}_2)\phi(x) + S_{12}\chi(x)]. \quad (7)$$

In the formulas the following notation is used: $x = mr$, where m is the average meson mass of the isomultiplet,

$$\phi(x) = \frac{e^{-x}}{x}$$

and

$$\chi(x) = \left(\frac{1}{3} + \frac{1}{x} + \frac{1}{x^2}\right)\frac{e^{-x}}{x}, \quad (8)$$

M denotes the proton mass, and M' denotes the

proton mass in pp and the neutron mass in np potentials.

(b) Vector-meson exchange. We have

$$H_V = ig_V\bar{\psi}\gamma_\mu\psi\phi_V^\mu + \frac{f_V}{4\mathfrak{M}}\bar{\psi}\sigma_{\mu\nu}\psi(\partial^\mu\phi_V^\nu - \partial^\nu\phi_V^\mu) \tag{9}$$

with

$$\sigma_{\mu\nu} = \frac{1}{2i}[\gamma_\mu, \gamma_\nu], \tag{10}$$

and $\mathfrak{M}$ denoting a scaling mass, which is chosen to be the proton mass, and

$$\begin{aligned} V_V = \frac{m}{4\pi}\Bigg\{ & \left[g_V^2\left(1+\frac{m^2}{8MM'}\right) + g_V f_V \frac{m^2}{2\mathfrak{M}(MM')^{1/2}} + f_V^2\frac{m^4}{16\mathfrak{M}^2MM'}\right]\phi(x) \\ & + \left[g_V^2\frac{m^2}{4MM'} + g_V f_V\frac{m^2}{2\mathfrak{M}(MM')^{1/2}} + f_V^2\frac{m^2}{4\mathfrak{M}^2}\left(1+\frac{m^2}{8MM'}\right)\right]\left[\tfrac{2}{3}(\vec{\sigma}_1\cdot\vec{\sigma}_2)\phi(x) - S_{12}\chi(x)\right] \\ & - \left[g_V^2\frac{3m^2}{2MM'} + g_V f_V\frac{2m}{\mathfrak{M}(MM')^{1/2}} + f_V^2\frac{3m^4}{8\mathfrak{M}^2MM'}\right]\left(\frac{1}{x}+\frac{1}{x^2}\right)\phi(x)\vec{L}\cdot\vec{S} \\ & + \left[g_V^2\frac{m^4}{16M^2M'^2} + g_V f_V\frac{m^4}{2\mathfrak{M}MM'(MM')^{1/2}} + f_V^2\frac{m^4}{2\mathfrak{M}^2MM'}\right]\frac{3}{x^2}\chi(x)Q_{12}\Bigg\}. \end{aligned} \tag{11}$$

(c) Scalar-meson exchange. We have

$$H_S = g_S\bar{\psi}\psi\phi_S \tag{12}$$

and

$$V_S = \frac{g_S^2}{4\pi}m\left[-\left(1-\frac{m^2}{8MM'}\right)\phi(x) - \frac{m^2}{2MM'}\left(\frac{1}{x}+\frac{1}{x^2}\right)\phi(x)\vec{L}\cdot\vec{S} - \frac{m^4}{16M^2M'^2}\frac{3}{x^2}\chi(x)Q_{12}\right]. \tag{13}$$

Effects of the width of a broad meson have been incorporated by replacing the propagator for a stable meson $1/(q^2+m^2)$ by[11,12]

$$P(q^2) = \left[q^2 + m^2 + \gamma\left(\frac{q^2}{m^2}\right)^n (q^2+4m_\pi^2)^{n+1/2}\right]^{-1}, \tag{14}$$

where

$$\gamma = m\Gamma/(m^2-4m_\pi^2)^{n+1/2} \tag{15}$$

with $n=0$ and 1 for ϵ and ρ, respectively.[22] This form has been chosen such that it has the following properties:

(i) It has a cut in the complex q^2 plane starting at the two-pion threshold $q^2 = -4m_\pi^2$ with the proper threshold behavior; and

(ii) it has a Breit-Wigner–type form in the neighborhood of $q^2 = -m^2$ with width Γ, due to the poles on the second Riemann sheet.

For both ϵ and ρ we write the propagator $P(q^2)$ as a dispersion integral,

$$P(q^2) = \int_{4m_\pi^2}^\infty \frac{\rho(m'^2)dm'^2}{q^2+m'^2}, \tag{16}$$

with

$$\rho(m'^2) = \frac{1}{\pi}\frac{\gamma(m'^2-4m_\pi^2)^{n+1/2}}{(m'^2-m^2)^2 + \gamma^2(m'^2/m^2)^{2n}(m'^2-4m_\pi^2)^{2n+1}}. \tag{17}$$

For the ρ meson ($n=1$) we needed in (14) an additional factor q^2/m^2 added to the term $(q^2+4m_\pi^2)^{3/2}$, which is responsible for the correct $|\vec{q}|^3$ threshold behaviour, in order to get rid of a pole of the propagator at the real axis in the first Riemann sheet, which would be present otherwise.[11] The superconvergent asymptotic behavior

$$P(q^2) \underset{q^2\to\infty}{\sim} (1/q^2)^{5/2} \quad \text{for } n=1 \tag{18}$$

leads to an additional pair of complex-conjugated spurious poles in the first Riemann sheet,

$$-\frac{A}{2}\left(\frac{1}{q^2+m_A^2 - im_A\Gamma_A} + \frac{1}{q^2+m_A^2+im_A\Gamma_A}\right), \tag{19}$$

which should be added to (16). The sum rules

$$\int_{4m_\pi^2}^\infty dm^2\rho(m^2) = A$$

and (20)

$$\int_{4m_\pi^2}^\infty dm^2m^2\rho(m^2) = m_A^2A$$

ensure that $P(q^2)$ decreases faster that $(1/q^2)^2$ for large q^2. We have looked numerically for the position of these spurious poles for the values of the ρ parameters,

$$m_\rho = 770 \text{ MeV}, \quad \Gamma_\rho = 146 \text{ MeV}, \tag{21}$$

obtaining

$$m_A = 680 \text{ MeV}, \quad \Gamma_A = 2150 \text{ MeV}. \tag{22}$$

The contributions of these spurious poles, which are very far from the region $q^2 = 0$, are neglected.

After taking the Fourier transform of (16) to configuration space, we obtain for a broad meson a superposition of Yukawa potentials with $2m'\rho(m'^2)$ as mass distribution. For practical reasons we have approximated such potentials by the sum of Yukawa potentials from two effective narrow mesons

$$\int_{2m_\pi}^{\infty} dm' 2m'\rho(m'^2)\frac{e^{-m'r}}{r} \simeq \beta_1 \frac{e^{-m_1 r}}{r} + \beta_2 \frac{e^{-m_2 r}}{r}. \tag{23}$$

For the ϵ meson we insert the values

$$m_\epsilon = 760 \text{ MeV}, \quad \Gamma_\epsilon = 640 \text{ MeV} \tag{24}$$

in order to have the ϵ pole in (14) at the same place as in the analysis of Protopopescu *et al.*[23]:

$$E(\epsilon) = 660 - i\,320 \text{ MeV}. \tag{25}$$

With the inputs (21) and (24) we approximate the "exact" potentials of the ρ and ϵ between $r = 0.3$–1.5 fm with the two-poles approximation of (23). The resulting values for β_i, m_i $(i = 1, 2)$ are given in Table I. The agreement is within 0.5% for both ϵ and ρ.

At short distances $r \lesssim 0.5$ fm the well-known needed strong repulsion is described phenomenologically by hard-core potentials. For a more extensive discussion, see Ref. 7. The radii of the hard cores will depend in general on the quantum numbers of the states $|J, L, S\rangle$. However, one introduces many phenomenological parameters this way. We have reduced the number of different hard-core radii, using the observation that almost all p and higher L waves are not very sensitive to hard-core variations. In particular we have for the p waves in NN that the $^1P_1$, $^3P_0$, and $^3P_1$ potentials are repulsive at distances $r \lesssim 0.5$ fm, and only the $^3P_2$ potential is attractive there. So we can just as well use one hard-core radius for all p waves, which is determined in fact by the $^3P_2$ phaseshifts. It turns out that we can use a single hard-core radius for the $L \geq 2$ waves, which are much less core-dependent. Only for too small values of the hard-core radius resonances or even bound states can occur easily. This way we end up with four hard-core radii in our NN model:

$$x_s \text{ for } {}^1S_0, \quad x_t \text{ for } {}^3S_1\text{-}{}^3D_1,$$
$$x_p \text{ for } L = 1, \text{ and } x_{L\geq 2} \text{ for } L \geq 2 \text{ waves}. \tag{26}$$

TABLE I. Values for the parameters in the two-poles approximation for the broad mesons ϵ and ρ. Masses and widths are given in MeV.

	n	m	Γ	β_1	m_1	β_2	m_2
ϵ	0	760	640	0.199 86	508.52	0.552 41	1043.79
ρ	1	770	146	0.158 74	628.74	0.783 21	878.18

In the case of the coupled $^3S_1$-$^3D_1$ waves we can just take one hard-core parameter needed for $^3S_1$, since the $^3D_1$ is very insensitive to the value of the hard-core radius. A similar reasoning applies to the coupled $^3P_2$-$^3F_2$ waves.

We note that an advantage of (26) is that the s waves do not influence the determination of the coupling constants too strongly because of the two s-wave cores. Therefore the coupling constants are mainly determined by the more peripheral waves.

III. RESULTS

The values of the 12 free parameters, 4 hard-core radii and 8 coupling constants, are searched by minimizing the total χ^2 with respect to the NN data. The χ^2 is calculated at $T_{\text{lab}} \approx 0$ by comparing the $^1S_0(pp)$ and $^3S_1(np)$ scattering lengths and effective ranges with their experimental values, and at $T_{\text{lab}} = 25$, 50, 95, 142, 210, and 330 MeV by comparing our calculated nuclear bar phase shifts with the NN energy-independent phase-shift analysis of the Livermore group,[15] i.e.,

$$\chi^2 = \sum_{i=0}^{6} \chi^2(T^i_{\text{lab}}). \tag{27}$$

In (27) $\chi^2(T^0_{\text{lab}})$ denotes the contribution of the low-energy parameters. $\chi^2(T^i_{\text{lab}})$ $(i = 1, \ldots, 6)$ is calculated by using the second-derivative matrices at each energy T^i_{lab} via the relation

$$\chi^2 = {\chi_{\min}}^2 + \sum_{kl} (\delta_k - \delta_k^{\text{exp}}) \frac{\partial^2 \chi^2}{\partial \delta_k \partial \delta_l} (\delta_l - \delta_l^{\text{exp}}), \tag{28}$$

where δ_k^{exp} denotes the set of phase shifts which give minimal χ^2 with respect to the experimental data: ${\chi_{min}}^2$. This way one gets for small deviations from δ_i^{exp} the true χ^2 compared to the experimental observables, since one takes into account the full correlations between the δ_k^{exp}.

The hard-core radii which emerged from the fit are

$$x_s = 0.521\,83 \text{ fm}, \quad x_t = 0.483\,95 \text{ fm},$$
$$x_p = 0.345\,94 \text{ fm}, \quad x_{L\geq 2} = 0.662\,54 \text{ fm}. \tag{29}$$

The obtained values for the coupling constants are given in Table II. For the $I = 0$ particles we

TABLE II. Meson-nucleon coupling constants from the fit to NN. The underlined couplings are constrained via SU(3). With the given figures the potential can be reproduced accurately.

	m (MeV)	$g/(4\pi)^{1/2}$	$f/(4\pi)^{1/2}$
π	138.041	3.660 00	
η	548.8	2.729 67	
X^0	957.5	3.887 86	
ρ	770 Γ=146	0.594 44	4.816 96
ϕ	1019.5	−1.124 12	−0.510 04
ω	783.9	3.373 08	2.339 92
ϵ	760 Γ=640	5.032 08	

give the couplings of the physical particles in cases of singlet-octet mixing. They are determined via fitting of unitary singlet couplings and employing the $F/(F+D)$ ratios α_V^e from theory or α_P from our YN analysis.[10]

In Table III we have listed the resulting nuclear bar phase shifts, and we have depicted them in Figs. 1–7. In Table IV we give the ^3L_C, ^3L_T, and $^3L_{LS}$ phase shifts[2] for $L=1, 2, 3$. Compared to the 1128 data used in the Livermore analysis up to 330 MeV, we obtain $\chi^2/\text{data}=2.37$.

At low energies the effective range expansion reads for $L=0, 1$

$$(1+\eta^2)^L p^{2L}[\,C_0^2(\eta)p\cot\delta+2\eta p h(\eta)] = -1/a+\tfrac{1}{2}rp^2-Pr p^4+\cdots, \quad (30)$$

where η, $C_0(\eta)$, and $h(\eta)$ are standard (see, e.g., Ref. 24). In the case of $^3P_2$ it is well known that there is an accidental p^5 low-energy behavior[24] due to one-pion exchange. In the Born approximation we have for the one-pion-exchange contribution (OPEC)

$$\delta^{\rm OPEC}(^3P_2) = -\frac{g^2(\pi)}{4\pi}\frac{p}{4E}\frac{1}{5}\left[Q_2\left(1+\frac{m_\pi^2}{2p^2}\right)-Q_1\left(1+\frac{m_\pi^2}{2p^2}\right)\right]$$

$$\simeq -\frac{g^2(\pi)}{4\pi}\frac{8}{15}\left(\frac{p}{m_\pi}\right)^5\frac{m_\pi}{M}+O\left(\frac{p^7}{m_\pi^7}\right) \quad (31)$$

in radians. Therefore we give for the $^3P_2$ wave the coefficients for the effective range expression, where the one-pion-exchange contribution has been subtracted[24]:

$$(1+\eta^2)p^2\{\,C_0^2(\eta)p\cot[\delta-\delta^{\rm OPEC}C_0^2(\eta)(1+\eta^2)]+2\eta p h(\eta)\} = -1/a+\tfrac{1}{2}rp^2+\cdots. \quad (32)$$

TABLE III. Nuclear bar pp and np phase shifts in degrees.

$T_{\rm lab}$ (MeV)	25	50	95	142	210	330
$^1S_0$	49.49	39.70	26.59	16.21	4.37	−11.59
$^3S_1$	80.12	61.94	43.47	30.86	17.72	1.43
ϵ_1	1.87	2.31	2.86	3.50	4.60	6.88
$^3P_0$	9.03	12.70	11.86	7.79	0.81	−10.97
$^3P_1$	−4.80	−8.11	−12.35	−15.93	−20.48	−27.47
$^1P_1$	−5.61	−7.77	−9.69	−11.35	−13.99	−19.09
$^3P_2$	2.31	5.53	10.24	13.27	15.37	15.92
ϵ_2	−0.78	−1.72	−2.78	−3.25	−3.28	−2.56
$^3D_1$	−2.78	−6.43	−11.83	−16.13	−20.75	−26.04
$^3D_2$	3.70	9.12	17.61	23.80	28.63	30.17
$^1D_2$	0.64	1.58	3.48	5.60	8.45	11.79
$^3D_3$	0.06	0.38	1.68	3.54	6.27	9.60
ϵ_3	0.54	1.59	3.32	4.69	6.01	7.16
$^3F_2$	0.10	0.32	0.74	1.10	1.40	1.22
$^3F_3$	−0.22	−0.66	−1.43	−2.08	−2.78	−3.70
$^1F_3$	−0.41	−1.11	−2.06	−2.66	−3.14	−3.61
$^3F_4$	0.02	0.10	0.39	0.84	1.66	3.29
ϵ_4	−0.05	−0.18	−0.49	−0.79	−1.17	−1.67
$^3G_3$	−0.05	−0.26	−0.86	−1.63	−2.81	−4.72
$^3G_4$	0.17	0.71	1.99	3.39	5.32	8.32
$^1G_4$	0.04	0.14	0.36	0.60	0.95	1.71
$^3G_5$	−0.01	−0.05	−0.15	−0.24	−0.26	0.03
ϵ_5	0.04	0.20	0.65	1.19	1.85	2.85
$^3H_4$	0.00	0.02	0.09	0.18	0.33	0.59
$^3H_5$	−0.01	−0.08	−0.27	−0.49	−0.80	−1.23
$^1H_5$	−0.03	−0.16	−0.49	−0.82	−1.21	−1.66
$^3H_6$	0.00	0.01	0.03	0.08	0.18	0.45
ϵ_6	−0.00	−0.02	−0.10	−0.20	−0.35	−0.59

The calculated s- and p-wave scattering lengths and effective ranges are compared to the experimental values in Table V.

The hard-core radius x_t in the $^3S_1-{}^3D_1$ waves has been fixed such that the experimental value for the binding energy of the deuteron is reproduced,

$$B=2.224\,644\ \text{MeV}. \quad (33)$$

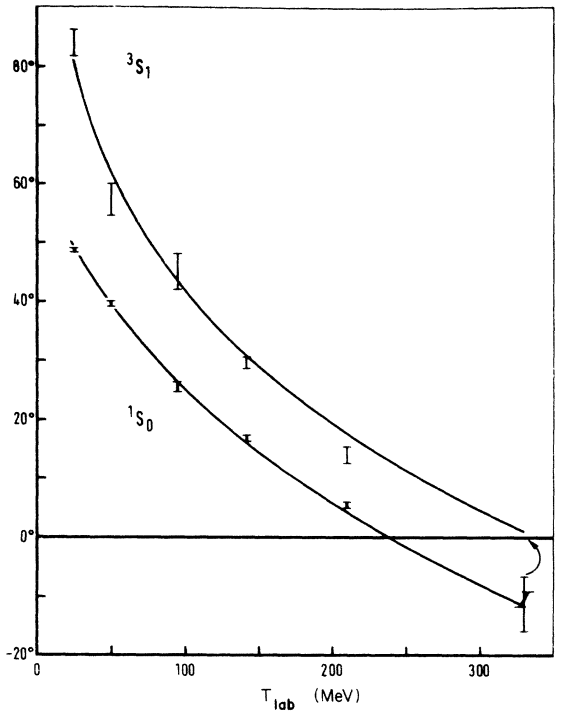

FIG. 1. $^1S_0(pp)$ and $^3S_1(np)$ nuclear bar phase shifts.

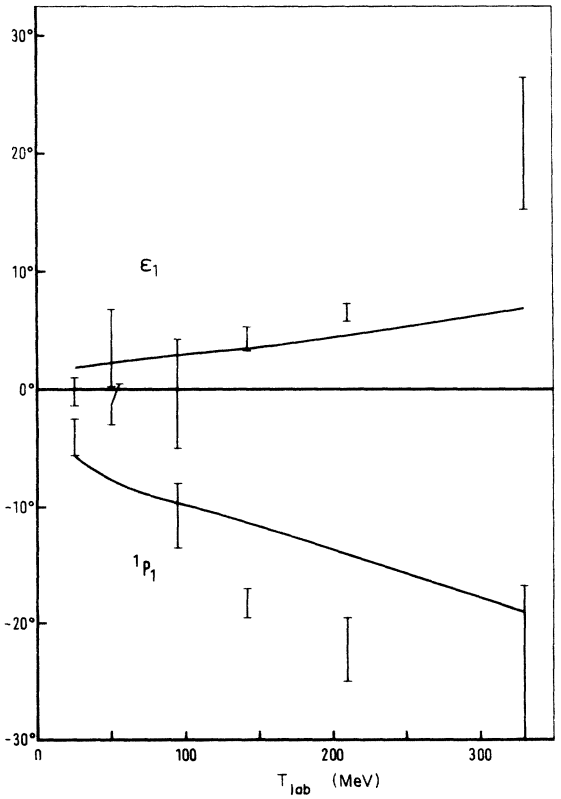

FIG. 2. $\epsilon_1(np)$ and $^1P_1(np)$ nuclear bar phase shifts.

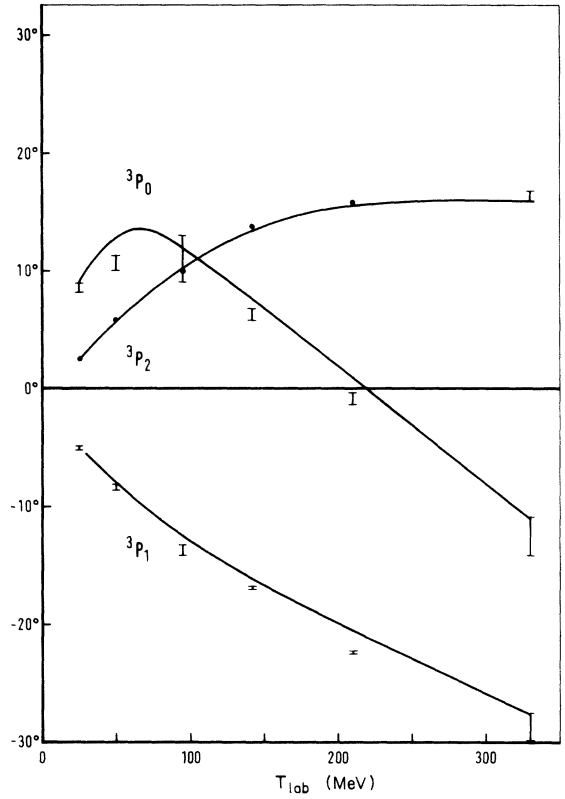

FIG. 3. $^3P_J(pp)$ $(J=0,1,2)$ nuclear bar phase shifts.

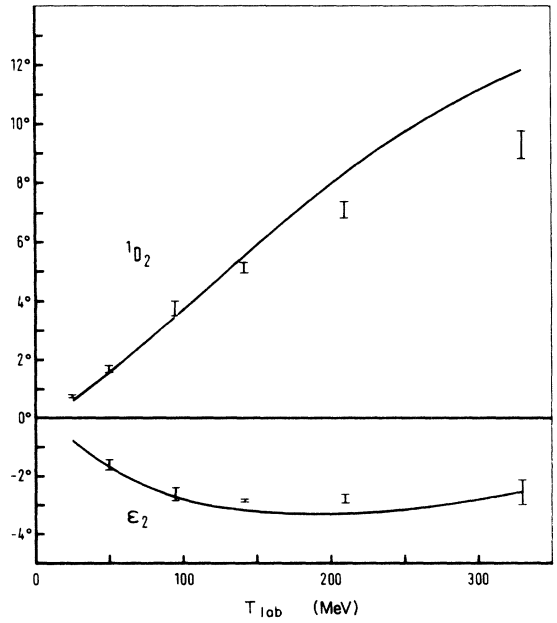

FIG. 4. $\epsilon_2(pp)$ and $^1D_2(pp)$ nuclear bar phase shifts.

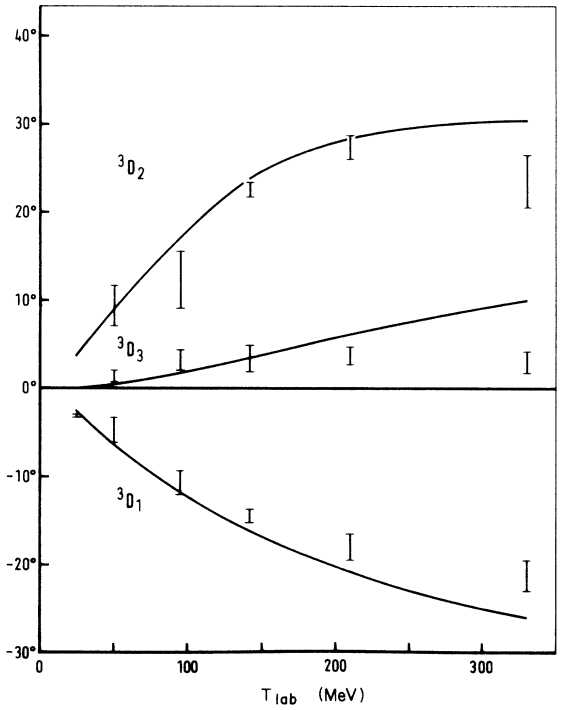

FIG. 5. $^3D_J(np)$ $(J=1,2,3)$ nuclear bar phase shifts.

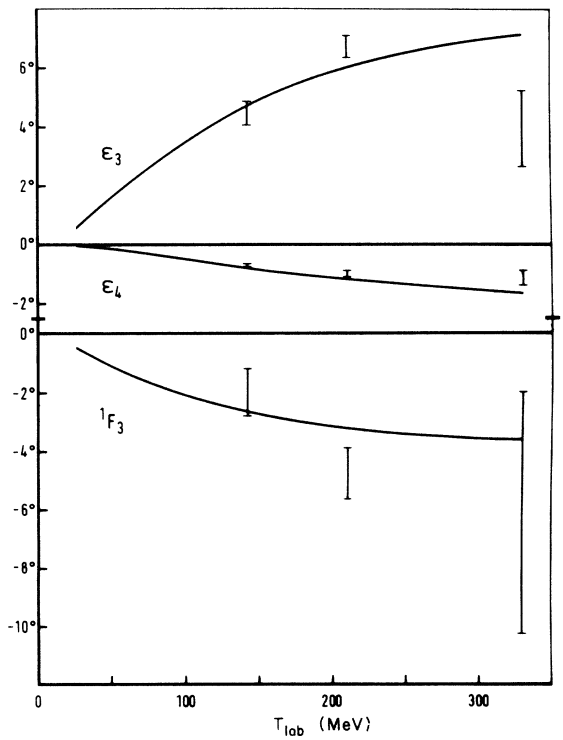

FIG. 6. $\epsilon_3(np)$, $\epsilon_4(pp)$, and $^1F_3(np)$ nuclear bar phase shifts.

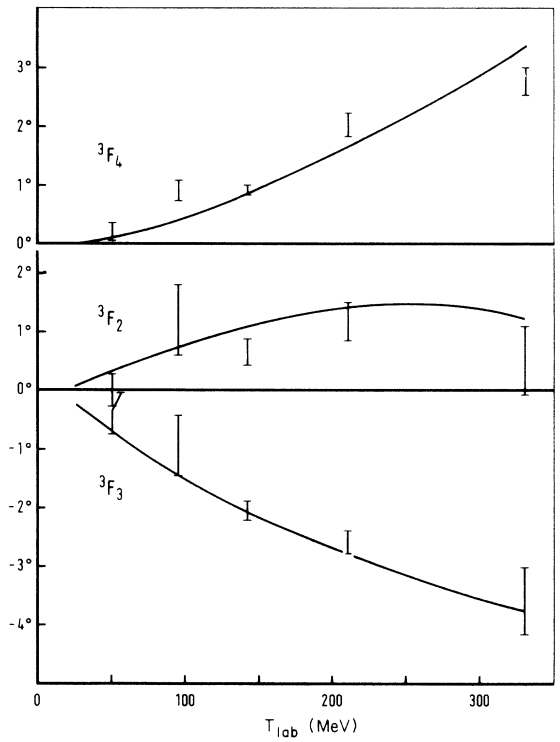

FIG. 7. $^3F_J(pp)$ $(J=2,3,4)$ nuclear bar phase shifts.

TABLE IV. ^3L_C, ^3L_T, and $^3L_{LS}$ phase shifts in degrees for $L=1,2,3$.

T_{lab} (MeV)	25	50	95	142	210	330
^3P_C	0.69	1.78	2.89	2.93	1.80	−1.53
^3P_T	−2.42	−3.84	−4.93	−5.32	−5.45	−5.30
$^3P_{LS}$	0.66	2.21	5.38	8.22	11.34	15.33
^3D_C	0.70	1.93	4.29	6.36	8.32	9.33
^3D_T	1.56	3.74	7.01	9.35	11.25	12.24
$^3D_{LS}$	0.12	0.29	0.70	1.26	2.19	3.63
^3F_C	−0.04	−0.10	−0.14	−0.07	0.12	0.47
^3F_T	−0.09	−0.28	−0.63	−0.96	−1.34	−1.82
$^3F_{LS}$	0.00	0.01	0.03	0.09	0.22	0.54

TABLE V. s- and p-wave effective range parameters in units of fm. Experimental values for the p waves are taken from Ref. 24.

	a	r	P	$a^{\exp}$	$r^{\exp}$
$^1S_0$	−7.814	2.670	0.0368	−7.823 ± 0.01	2.794 ± 0.015
$^3S_1$	5.431	1.771	−0.0084	5.423 ± 0.005	1.761 ± 0.005
$^3P_0$	−3.042	3.336	−0.0065	−2.6 ± 2.0	4.3 ± 2.0
$^3P_1$	1.828	−7.463	−0.0006	2.8 ± 1.3	−9.0 ± 1.0
$^3P_2$	−0.270	4.561	−0.0113	−0.45 ± 0.28	15 ± 10
$^1P_1$	2.397	−7.139	−0.0019		

In Table VI the results for the deuteron parameters are given: the d-state probability P_d, the electric quadrupole moment Q, the deuteron effective range $\rho(-B, -B)$, the asymptotic normalization $N_g{}^2$, and the s-d admixture $A = \tan\epsilon_g$ (for definitions see Ref. 25). The deuteron wave functions are listed in Table VII, and they are drawn and compared to Reid's wave functions[16] in Fig. 8.

IV. DISCUSSION

A. Coupling constants

The value $g^2(\pi)/4\pi = 13.40$ is more than two standard deviations smaller than the result of the 26 parameter solution in the NN analysis of the Livermore group,[15] $g^2(\pi)/4\pi = 14.43 \pm 0.41$. Similarly our value $f^2(\pi)/4\pi = 0.0725$ is two standard deviations away from the preferred value from πN analyses[26] $f^2(\pi)/4 = 0.081^{+0.003}_{-0.004}$. The most recent πN dispersion relation analyses[26] seems to give systematically lower values than $f^2(\pi)/4\pi = 0.081$. The discrepancy with our value can be covered at least partially by the observation that we have approximated $g^2(\pi)/4ME$ in the derivation of OPEP (Ref. 20) by $g^2(\pi)/4M^2$. This means that we should compare our value perhaps with (M/E) $g^2(\pi)/4\pi$ (Table VIII). Because the more peripheral waves have only entries in the phase-shift analyses at the higher energies, one expects beforehand to obtain in our analysis a value for $g^2(\pi)$ lower than the actual value. Also the d waves try to depress the value of $g^2(\pi)$ (see Sec. IV B). On the other hand, at very low energies the π coupling becomes too small, which influences strongly the effective ranges and deuteron parameters (see Sec. IV C). We have made a compromise in the sense that we have fixed $g(\pi)$ such that a_t and r_t are roughly one standard deviation from their experimental values (Table V), thereby keeping the binding energy of the deuteron at the correct value.

The physical particles η and X^0 are mixtures of the pure octet state η_8 and the pure singlet state X_1^0. We use the mixing angle from the Gell-Mann–Okubo mass formula $\theta_P = -10.4°$, which is consistent with experiment.[27] The η and X^0 are difficult to separate in NN, because the fit is mainly sensitive to g^2/m^2 and not much to the particular g^2 and m^2 separately. Various combinations of $g(\eta)$ and $g(X^0)$ can give the same χ^2 after readjustment of the hard-core radii. The virtue of a combined NN and YN analysis is that we can fix the octet coupling $g^8(\eta)$ via SU(3) using the value of $\alpha_P = F/(F+D)$ from the YN analysis, which is at some points very sensitive to α_P. In the fit to NN we have to determine still one parameter for both η and X^0: the singlet coupling constant $g^1(X^0)$. With the value[10]

$$\alpha_P = 0.485 \pm 0.012 \tag{34}$$

we arrive at $g^2(\eta)/4\pi = 7.45$ and $g^2(X^0)/4\pi = 15.12$. The ratio $g^2(\eta)/g^2(\pi) = 0.56$ is in good agreement with the η/π^0 ratio 0.45 ± 0.11 resulting from counter data on backward $\pi^- p \to \eta n$ and $\pi^- p \to \pi^0 n$ at 6 GeV/c.[28] In the analysis of the reaction $p + d \to \mathrm{He}^3 + MM$ at 2.8 and 3.8 GeV/c Odorico gives the estimates[29] $g^2(\pi):g^2(\eta):g^2(X^0)$ $= 1:0.75 \pm 0.03:0.4 \pm 0.02$. However, there are many uncertainties in his analysis. These ratios lead to a very large mixing angle, e.g., $\theta_P \simeq -35°$ for $\alpha_P = 0.4$, and still $\theta_P \lesssim -20°$ for α_P given in (34).

The direct ρ coupling[33] $g^2(\rho)/4\pi = 0.353$ seems

TABLE VI. Calculated deuteron parameters. For definitions see Ref. 25.

P_d	Q	$\rho(-B, -B)$	$N_g{}^2$	A
5.92%	0.2721 fm^2	1.776 fm	0.7868 fm	0.0251

TABLE VII. Deuteron wave functions in $\mathrm{fm}^{-1/2}$. u and w are the wave functions for $^3S_1$ and $^3D_1$, respectively.

r (fm)	$u(r)$	$w(r)$	r (fm)	$u(r)$	$w(r)$
0.483 95	0.0	0.0	3.007 01	0.432 73	0.093 65
0.605 46	0.134 10	0.069 61	3.207 14	0.414 92	0.085 22
0.705 53	0.230 96	0.106 73	3.407 27	0.397 46	0.077 58
0.805 59	0.311 04	0.132 23	3.607 40	0.380 45	0.070 68
0.905 65	0.374 52	0.150 18	3.807 53	0.363 98	0.064 45
1.005 72	0.423 29	0.162 49	4.007 66	0.348 07	0.058 83
1.105 78	0.459 72	0.170 31	4.493 68	0.311 87	0.047 36
1.205 85	0.486 10	0.174 52	5.008 30	0.277 32	0.037 94
1.305 91	0.504 45	0.175 85	5.522 92	0.246 42	0.030 65
1.405 98	0.516 47	0.174 96	6.037 54	0.218 87	0.024 95
1.506 04	0.523 51	0.172 40	6.494 98	0.196 94	0.020 91
1.606 10	0.526 68	0.168 60	7.009 60	0.174 86	0.017 25
1.706 17	0.526 85	0.163 94	7.524 21	0.155 23	0.014 31
1.806 23	0.524 68	0.158 68	8.038 83	0.137 81	0.011 95
1.906 30	0.520 72	0.153 05	8.496 27	0.123 96	0.010 21
2.006 36	0.515 39	0.147 22	9.010 89	0.110 04	0.008 60
2.206 49	0.501 82	0.135 41	10.040 12	0.086 70	0.006 16
2.406 62	0.485 83	0.123 88	11.012 18	0.069 23	0.004 55
2.606 75	0.468 55	0.113 00	12.041 42	0.054 54	0.003 32
2.806 88	0.450 69	0.102 90	13.013 47	0.043 55	0.002 47

to be rather small. The assumption of universal coupling of the ρ to the isospin current[14] and the vector dominance model (VDM) for the electromagnetic current leads to numerous estimates[30] of $g(\rho)$ yielding all values in the band $0.5 \lesssim g^2(\rho)/4\pi \lesssim 0.7$. In particular the assumption of ρ dominance for the isovector electric form factor of the nucleon leads to the equality

$$g^2(\rho)/4\pi \approx \gamma^2(\rho)/4\pi, \tag{35}$$

where γ_ρ denotes the ρ-photon coupling constant. This coupling has been determined rather ac-

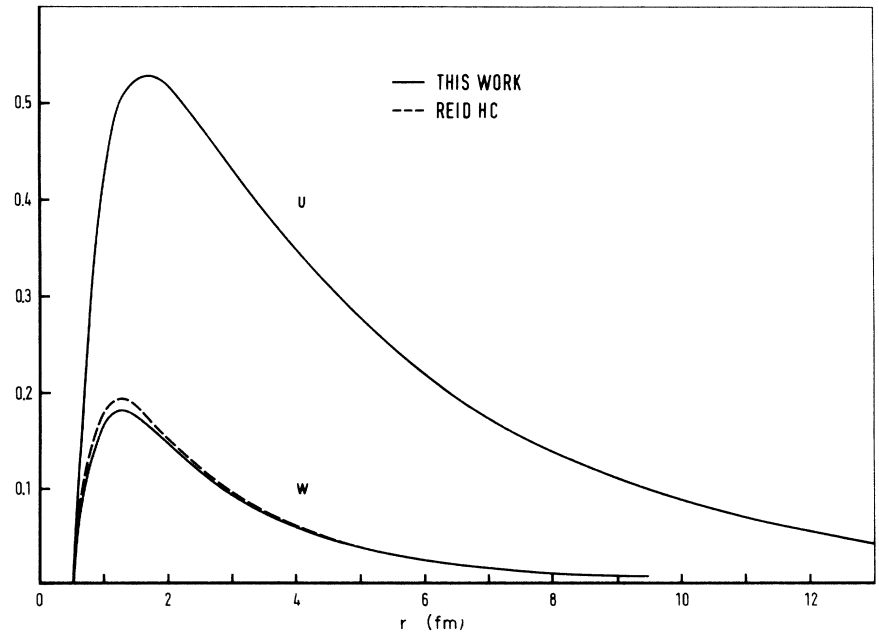

FIG. 8. The deuteron wave functions u and w. For comparison, Reid's (hard-core) (Ref. 16) deuteron wave functions are also drawn.

TABLE VIII. Pion effective couplings strengths at various energies. At energy 0 the value of the *NN* phase-shift analysis (Ref. 15) is used as input.

T_{lab} (MeV)	0	25	50	95	142	210	330
$(M/E)g^2(\pi)/4\pi$	14.43	14.33	14.24	14.08	13.91	13.66	13.27

curately in e^+e^- colliding-beam experiments[31], yielding $\gamma^2(\rho)/4\pi = 0.58 \pm 0.06$. However, total hadronic photoabsorption cross sections and vector-meson photoproduction lead to smaller values of $\gamma^2(\rho)/4\pi$, even when the ρ' is included.[32] Furthermore, in (35) there is in principle also some contamination of the recently discovered ρ', which has the same quantum numbers as the ρ. It is interesting to compare the values of the direct ρ couplings[33] and the δ couplings for the various analyses in the compilation.[26] A simultaneous occurrence of both smaller or both larger ρ and δ couplings becomes apparent. The explanation may be found in the fact that the central potentials of the ρ and δ cancel each other largely, whereas the spin-orbit potentials reinforce each other, although being much smaller than the strong spin-orbit forces of the ω and ϵ (see below). Since we neglect the δ completely in this model, we expect to find a low value for $g(\rho)$. We may draw the conclusion that the direct ρ coupling is not very well determined in *NN* analyses.

The value $f(\rho)/(4\pi)^{1/2} = 4.82$ is slightly larger than most *NN* analyses[26] give, having values $\gtrsim 4$. The ratio $f(\rho)/g(\rho) = 8.10$ expresses the repercussion of our small value of $g(\rho)$. Most *NN* analyses have values for this ratio $f(\rho)/g(\rho) \gtrsim 5$, which are larger than 3.7 as expected from ρ dominance of the isovector electromagnetic form factors when the ρ' is neglected completely. Values of about 7 for this ratio are obtained in πN dispersion relations.[26,33]

The ω and ϕ coupling constants are discussed together, since they are related via SU(3). Consequently the signs are determined as well. Our convention for the physical ω and ϕ states involving the ideal mixing angle $\theta_V = \arctan(1/\sqrt{2})$ reads

$$|\omega\rangle = (\tfrac{2}{3})^{1/2}|\omega_1\rangle + (\tfrac{1}{3})^{1/2}|\phi_8\rangle ,$$
$$|\phi\rangle = -(\tfrac{1}{3})^{1/2}|\omega_1\rangle + (\tfrac{2}{3})^{1/2}|\phi_8\rangle , \tag{36}$$

where $|\omega_1\rangle$ denotes the unitary singlet and $|\phi_8\rangle$ the octet isoscalar. With the theoretical input $\alpha_V^e = 1$ for the direct coupling the three coupling constants $g(\rho)$, $g(\omega)$, and $g(\phi)$ are determined by searching $g(\rho)$ and $g^1(\omega)$. We find opposite signs for $g(\omega)$ and $g(\phi)$ (Table II). This leads to an excellent agreement with VDM for the isoscalar electric form factor of the nucleon. VDM gives the relation

$$F_1^S(t) = \frac{g_{\omega NN}/2\gamma_\omega}{1 - t/m_\omega^2} + \frac{g_{\phi NN}/2\gamma_\phi}{1 - t/m_\phi^2} , \tag{37}$$

where $t = -q^2$, and the normalization condition reads

$$F_1^S(0) = \tfrac{1}{2}. \tag{38}$$

The photo-vector meson couplings are rather well known,[34]

$$\gamma_\omega^2/4\pi = 4.6 \pm 0.45, \quad \gamma_\phi^2/4\pi = 3.6 \pm 0.3. \tag{39}$$

SU(3) symmetry together with ideal mixing leads in our convention to the relation

$$\gamma_\rho : \gamma_\omega : \gamma_\phi = \tfrac{1}{3} : 1 : 1/\sqrt{2} . \tag{40}$$

Inserting our values for the *NN* coupling constants (Table II) together with γ_ω and γ_ϕ from (39) with the signs as predicted by SU(3), we have at $t = 0$

$$F_1^S(0) = \frac{g_{\omega NN}}{2\gamma_\omega} + \frac{g_{\phi NN}}{2\gamma_\phi} = 0.48 \pm 0.04, \tag{41}$$

which is to be compared with (38).

The derivative couplings of the vector mesons $f(\rho)$ and $f(\omega)$ are very well fixed in the *NN* search. Unfortunately, we do not have in this case such a firm theoretical value for α_V^m as in the case of the direct couplings for α_V^e. Therefore $f(\phi)$ is searched too in *NN* in spite of its smaller sensitivity. In fact, varying $f(\phi)/(4\pi)^{1/2}$ between -0.3 and -0.9 (which corresponds to $0.34 > \alpha_V^m > 0.30$), the χ^2/data changes only 0.1. Since α_V^m is not too well determined in *NN* via $f(\rho)$, $f(\omega)$, and $f(\phi)$, we have checked its value by searching it in *YN*, thereby keeping $f_{\rho NN}$ and $f_{\omega NN}$ fixed. The result is[10]

$$\alpha_V^m = 0.334 \pm 0.035, \tag{42}$$

indicating the same order of uncertainty as in *NN*. We note that the searched derivative couplings of ω and ϕ have the same signs as the direct ones and hence have opposite signs. The isoscalar magnetic form factor of the nucleon requires at $t = 0$

$$F_2^S(0) = \tfrac{1}{2}(\kappa_p + \kappa_n) = -0.06, \quad (43)$$

where κ_p and κ_n denote the anomalous magnetic moments of the proton and the neutron.

For our values of $f(\omega)$ and $f(\phi)$ (Table II), using (39) and the signs as predicted by SU(3) we obtain from naive VDM

$$F_2^S(0) = \frac{f_{\omega NN}}{2\gamma_\omega} + \frac{f_{\phi NN}}{2\gamma_\omega} = 0.41 \pm 0.03; \quad (44)$$

i.e., the test fails. The agreement for the isoscalar electric form factor and the failure for the magnetic one may be inderstood in the light of the Siegert theorem,[35] which states that electric moments can be calculated reliably, whereas for magnetic moments such a theorem does not exist. The formula (44) may therefore be much too simplistic. Both the ϕ couplings are much smaller than the ω couplings (Table II). This is compatible with the observation of a backward peak in $K^- p \to \Lambda\omega$ and almost no events in the backward hemisphere in $K^- p \to \Lambda\phi$.

The coupling constants $g(\epsilon)$ and $g(\omega)$ are mainly determined via the collaboration that together they build up the strong spin-orbit force needed to separate the ${}^3P_{0,1,2}$ waves, while the central attraction of the ϵ and the central repulsion of the ω cancel each other largely. Above, we noticed that our $g(\omega)$ has a realistic value. However, the ϵNN coupling is much harder to guess from other work. Petersen and Pišut[36] obtain in an analysis of $\pi\pi \to N\bar{N}$ and $\pi\pi \to \pi\pi$ (inserting the "between-up, up-down, down-down" solutions for the $\pi\pi$ $I=0$ s-wave phase shift, which seem to be the most reasonable ones experimentally) the ratio

$$\frac{g_{\epsilon NN}}{g_{\epsilon\pi\pi}} = (1.8 \pm 0.5)\, m_\pi^{-1}. \quad (45)$$

When we try to estimate $g_{\epsilon\pi\pi}$ in the narrow-width approximation from the pole parameters (25) we obtain

$$\frac{g_{\epsilon\pi\pi}^2}{4\pi} \approx 16\, m_\pi^2. \quad (46)$$

Combining (45) and (46) leads to

$$\frac{g_{\epsilon NN}}{(4\pi)^{1/2}} = 7.2 \pm 2.0, \quad (47)$$

which agrees with our result (Table II). In field-theoretical calculations of uncorrelated 2π exchange (TPEP)[37] one obtains a spin-orbit potential of reasonable magnitude and of the same sign as the ω and ϵ contributions. If TPEP is an important contribution to the nuclear potential, it will probably depress $g(\epsilon)$ and possibly also $g(\omega)$. Therefore we conclude that such high values of the direct ω coupling as one uses in photoproduction, electroproduction, and weak pion production[38] would cause a disaster in NN.

B. The ϵ_1 and ${}^3D_2$ phases

The simultaneous fit to the ϵ_1 and ${}^3D_2$ phases poses one of the major problems for potential models. For a review see Ref. 16, where phenomenological potentials of the form

$$V = V_C + V_\sigma \vec{\sigma}_1 \cdot \vec{\sigma}_2 + V_T S_{12} + V_{SO} \vec{L} \cdot \vec{S} \quad (48)$$

are examined.

In Table IX we compare the ϵ_1 and ${}^3D_2$ phase shifts of this work and of the recent work of Bryan and Gersten (BG)[6] with the Livermore phase shifts. Most meson-theoretical models obtain too small values for ϵ_1 at 210 and 330 MeV.[3] We obtain good values for ϵ_1 just as the BG model[6] and the OBEP model of Holinde, Erkelenz, and Alzetta (HEA).[39]

In Table IX we notice that the models of Ref. 6 predict too high ${}^3D_2$ phases. The same remark applies to the HEA model. It is well known that the ${}^3D_2$ phase shift from OPEP alone grows above

TABLE IX. Comparison of the ${}^3D_2$ and ϵ_1 phase for several OBE models and the Livermore phase-shift analysis (Ref. 15).

	${}^3D_2$			ϵ_1		
T_{lab} (MeV)	50	142	330	50	142	330
This work	9.12	23.80	30.17	2.31	3.50	6.88
BS IV[a]	10.34	28.37	37.92	2.10	2.56	3.76
BG	10.37	27.60	34.11	2.78	4.73	8.66
Livermore X	9.36 ± 2.24	22.54 ± 0.79	23.44[b] ± 3.01	3.53 ± 3.27	4.28 ± 0.96	20.93[b] ± 5.63

[a] Updated version of BS III (Ref. 40) published together with the BG model in Ref. 6.

[b] Alternative solution of the Livermore analysis [M. H. Mac Gregor, R. A. Arndt, and R. M. Wright, Phys. Rev. 173, 1272 (1968)]: $\delta({}^3D_2) = 17.27 \pm 2.18$ and $\epsilon_1 = 7.24 \pm 2.63$.

60° at 330 MeV. Therefore one has to damp the OPEP strongly in OBEP models. The phenomenological Hamada-Johnston[18] and Yale[19] potentials have a strong quadratic spin-orbit potential V_Q mainly to depress the $^3D_2$ phase. However, it seems that such a strong quadratic spin-orbit force as in Ref. 18 and 19 cannot be produced by the ρ, ω, ϕ, and ϵ. Although our $^3D_2$ phases are rather good (cf. Table IX), our model does not provide a genuine solution to the $^3D_2$ problem, since the $^3D_2$ phases are suppressed also phenomenologically by the large $x_{L\geq 2}$ core.

The BS IV (Bryan-Scott) model (updated BS III[40]),[6] which has momentum dependence in V_C but not a V_Q potential, gives only slightly higher $^3D_2$ phase shifts than the BG model (Table IX). However, their ϵ_1 is too small at higher energies. The BG model[6] using the Blankenbecler-Sugar equation differs substantially from BS IV only for its good ϵ_1 and having at the same time lower $^3D_2$ phases (Table IX) but still significantly too high. Note that the BG model is evaluated in momentum space and so it contains implicitly energy dependence and quadratic spin-orbit effects. The situation in the HEA model[39] is similar. Therefore we may conclude that the inclusion of momentum dependence in the potentials may improve things a little, but does not solve the problem in the $^3D_2$ wave.

Finally, we want to remark that one-pion exchange (OPE) treated by geometric unitarization yields lower OPE phases,[12] but also in such an approach the problem persists.

C. Hard cores and low-energy parameters of s and p waves

Our model has 3 s and p hard-core parameters. For waves with $L=1$ one core was necessary, mainly determined by the $^3P_2$ wave. For the s waves we have introduced two hard cores in order to obtain a close fit to the low-energy parameters and the phase-shift analysis. Physically this is quite acceptable, since the $^1S_0$ and $^3S_1$ states differ in spin, isospin, and SU(3) representation. Therefore imaginable contributions to the short-range repulsion, such as, e.g., relativistic effects (multiparticle states) or heavy mesons, are different for $^1S_0$ and $^3S_1$. The BG model and BS IV model[6] employ one cutoff parameter only. Their results for the low-energy parameters naturally come out worse than ours, but are not bad at all. Taking only one s-wave hard core in our model and adjusting the coupling constants [mainly $g^1(X^0)$], also gives good low-energy parameters and almost the same χ^2. The main reason we used 2 s-wave hard cores is to avoid as much bias as possible in the determination of the coupling constants due to the short-range parametrization. For comparison we have shown the $^3S_1$ low-energy parameters of various models in Table X together with the experimental values.

We note that in our model the hard core x_t in the $^3S_1$-$^3D_1$ waves has been fixed such as to reproduce the experimental value of the deuteron binding energy B. The values of a_t and r_t are determined then. They turn out to be about two standard deviations higher than their experimental values.

Our value for the electric quadrupole moment Q of the deuteron is too low. The sensitivity of Q to parameter variations is by far the largest with respect to $g(\pi)$, even such that it may be used as a tool to determine $g(\pi)$ very accurately. Therefore our low Q value is a consequence of the low value of $g(\pi)$. Raising $g(\pi)$ to $g^2(\pi)/4\pi = 14.43$ yields, after readjustment of the hard-core radii, the values of Table XI for the low-energy parameters. Q turns out to be all right now, but because of the larger value of r_t in this case, a_t needs to be larger too in order to reproduce B. We have fixed $g(\pi)$ such that B exactly has and a_t almost has its experimental value (see Table X).

The larger value of $g(\pi)$ raises also the effective range r_s in the $^1S_0(pp)$, but it remains still 5 standard deviations lower than its experimental value.[41]

TABLE X. Comparison with experiment of the $^3S_1$ low-energy parameters and the binding energy B and the electric quadrupole moment Q of the deuteron for several OBE models.

	a_t (fm)	r_t (fm)	B (MeV)	Q (fm^2)
Experiment [a,b]	5.423 ± 0.005	1.761 ± 0.005	2.224 644 ± 0.000 046	0.2875 ± 0.002
This work	5.431	1.771	2.224 644	0.2721
BS IV [c,d]	5.41	1.84	2.24	0.277
BG [c]	5.39	1.81		

[a] a_t, r_t, B from Ref. 41.
[b] Q from R. V. Reid, Jr. and M. L. Vaida, Phys. Rev. Lett. 29, 494 (1972).
[c] Ref. 6.
[d] a_t, r_t, and B inconsistent with effective range formula.

TABLE XI. Low-energy parameters, calculated with $g^2(\pi)/4\pi = 14.43$.

	$^1S_0(pp)$	$^3S_1$	$^1P_1$	$^3P_0$	$^3P_1$	$^3P_2$
a	−7.833	5.466	2.577	−3.333	1.966	−0.282
r	2.721	1.817	−6.677	2.966	−6.970	4.215
P	0.0366	−0.0106	−0.0022	−0.0080	−0.0006	−0.0111

B	P_d	Q	$\rho(-B,-B)$	N_g^2	A
2.224 644	6.25%	0.2878 fm^2	1.818 fm	0.8001 fm	0.0265

In the latest pp phase-shift analysis[42] lower values of r_s are also obtained: $r_s = 2.687 \pm 0.015$ fm or $r_s = 2.669 \pm 0.009$ fm. The only difference with Ref. 41 in the low-energy experimental input set used consists of not taking the datum at 382.43 keV (Ref. 43) in the latter analysis. At the same time, of course, slightly different values of a_s are also obtained: $a_s = -7.761 \pm 0.010$ fm or $a_s = -7.745 \pm 0.007$ fm, respectively. These could be obtained easily in our model by changing x_s slightly.

In Table IV we have also displayed the calculated p-wave effective range parameters. From Table XI one can get some feeling about the model dependence. The $^3P_{0,1,2}$ scattering lengths and effective ranges agree best with set III of Sher, Signell, and Heller[26], i.e., the analysis where the Wisconsin and Berkeley data are omitted.

ACKNOWLEDGMENTS

We would like to thank Dr. A. Gersten for many illuminating discussions about the nucleon-nucleon problem and for making his fitting procedures available to us. Discussions with Professor R. Vinh Mau and Professor H. P. Noyes are gratefully acknowledged.

Part of this work was included in the research program of the Stichting voor Fundamenteel Onderzoek der Materie (F.O.M.) with financial support from the Nederlandse Organisatie voor Zuiver-Wetenschappelijk Onderzoek (Z.W.O.)

†FOM research associate.

[1]S. Ogawa, S. Sawada, T. Ueda, W. Watari, and M. Yonezawa, Prog. Theor. Phys. Suppl. 39, 140 (1969).

[2]P. Signell, in *Advances in Nuclear Physics*, edited by M. Baranger and E. Vogt (Plenum, New York, 1969), Vol. 2. p. 223.

[3]P. Signell, in *Few Particle Problems in the Nuclear Interaction*, pag. 1, edited by I. Slaus, S. A. Moszkowski, R. P. Haddock, and W. T. H. Van Oers (North-Holland, Amsterdam, 1972), p. 1.

[4]M. Moravcsik, Rep. Prog. Phys. 35, 587 (1972).

[5]See Particle Data Group, Rev. Mod. Phys. 43, S1 (1971), or later versions.

[6]R. A. Bryan and A. Gersten, Phys. Rev. D 6, 341 (1972).

[7]M. M. Nagels, T. A. Rijken, and J. J. de Swart, Ann. Phys. (N. Y.) 79, 338 (1973).

[8]M. M. Nagels, T. A. Rijken, and J. J. de Swart, in *Few Particle Problems in the Nuclear Interaction*, edited by I. Slaus, S. A. Moszkowski, R. P. Haddock, and W. T. H. Van Oers (Ref. 3), p. 42.

[9]M. M. Nagels, T. A. Rijken, and J. J. de Swart, Phys. Rev. Lett. 31, 569 (1973).

[10]M. M. Nagels, T. A. Rijken, and J. J. de Swart, Univ. of Nijmegen, Nijmegen, The Netherlands, report (unpublished).

[11]J. Schwinger, Phys. Rev. D 3, 1967 (1971).

[12]J. Binstock and R. A. Bryan, Phys. Rev. D 4, 1341 (1971).

[13]A. Gersten, R. H. Thompson, and A. E. S. Green, Phys. Rev. D 3, 2076 (1971).

[14]J. J. Sakurai, Ann. Phys. (N. Y.) 11, 1 (1960).

[15]M. H. Mac Gregor, R. A. Arndt, and R. M. Wright, Phys. Rev. 182, 1714 (1969).

[16]R. V. Reid, Ann. Phys. (N. Y.) 50, 411 (1968).

[17]J. J. de Swart, M. M. Nagels, T. A. Rijken, and P. A. Verhoeven, *Springer Tracts in Modern Physics*, edited by G. Höhler (Springer, New York, 1971), Vol. 60, p. 138.

[18]T. Hamada, and I. D. Johnston, Nucl. Phys. 34, 382 (1962).

[19]K. E. Lassila, M. H. Hull, Jr., H. M. Ruppel, F. A. McDonald, and G. Breit, Phys. Rev. 126, 881 (1962).

[20]M. M. Nagels, Ph.D. thesis, Univ. of Nijmegen, Nijmegen, The Netherlands (unpublished).

[21]N. Hoshizaki, and S. Machida, Prog. Theor. Phys. 24, 1325 (1960).

[22]Such a representation for $I = 0$ and $I = 1$ low-energy $\pi\pi$ scattering would lead to the values for the scattering lengths and effective ranges $a_0^0 = 0.38 m_\pi^{-1}$, $r_0^0 = -0.80 m_\pi^{-3}$, $a_1^1 = 0.002 m_\pi^{-3}$. Comparison with the literature (see Ref. 26) shows that this ϵ representation describes the interaction in the $I = 0$ s wave near the $\pi\pi$-threshold well, whereas for the $I = 1$ p wave the ρ seems to give a less complete description.

[23]S. D. Protopopescu, M. Alston-Garnjost, A. Barbaro-Galtieri, S. M. Flatté, J. H. Friedman, T. A. Lasinski,

G. R. Lynch, M. S. Rabin, and F. T. Schmitz, Phys. Rev. D 7, 1279 (1973).
[24]M. S. Sher, P. Signell, and L. Heller, Ann. Phys. (N. Y.), 58, 1 (1970).
[25]L. Hulthén and M. Sugawara, in *Handbuch der Physik*, edited by S. Flügge (Springer, Berlin, 1957), Vol. 39, p. 1.
[26]H. Pilkuhn, W. Schmidt, A. D. Martin, C. Michael, F. Steiner, B. R. Martin, M. M. Nagels, and J. J. de Swart, Nucl. Phys. B65, 460 (1973).
[27]A. Duane, D. M. Binnie, L. Camilleri, J. Carr, N. C. Debenham, D. A. Garbutt, W. G. Jones, J. Keyne, I. Siotis, and J. G. McEwen, Phys. Rev. Lett. 32, 425 (1974).
[28]J. D. Boright, D. R. Bowen, D. E. Groom, J. Orear, D. P. Owen, A. J. Pawlicki, and D. H. White, Phys. Lett. 33B, 615 (1970).
[29]R. Odorico, Phys. Rev. D 8, 3080 (1973).
[30]J. J. Sakurai, *Boulder Lectures in Theoretical Physics: Vol XI-A, Elementary Particle Physics*, edited by W. E. Britten *et al.* (Gordon and Breach, New York, 1968), p.1.
[31]D. Benaksas, G. Cosme, B. Jean-Marie, S. Jullian, F. Laplanche, J. Lefrançois, A. D. Liberman, G. Parrour, J. P. Reppelin, and G. Sauvage, Phys. Lett. 39B, 289 (1972).
[32]G. Wolf, DESY Report No. DESY 72/61 (unpublished).
[33]Our direct ρ coupling differs by a factor of $\frac{1}{2}$ compared to Sakurai's convention (See Ref. 14) and the convention in πN dispersion relations (see Ref. 26).
[34]D. Benaksas, C. Cosme, B. Jean-Marie, S. Jullian, F. Laplanche, J. Lefrançois, A. D. Liberman, G. Parrour, J. P. Reppelin, and G. Sauvage, Phys. Lett. 42B, 507 (1972); C. Cosme, B. Jean-Marie, S. Jullian, F. Laplanche, F. Lefrançois, A. D. Liberman, G. Parrour, J. P. Reppelin, and G. Sauvage, Phys. Lett. 48B, 155 (1974).
[35]R. G. Sachs, *Nuclear Theory* (Addison-Wesley, Reading, Mass., 1953).
[36]J. L. Petersen and J. Pišut, Nucl. Phys. B38, 207 (1972).
[37]M. H. Partovi and E. L. Lomon, Phys. Rev. D 2, 1999 (1970).
[38]F. A. Berends, A. Donnachie, and D. L. Weaver, Nucl. Phys. B4, 103 (1967); J. D. Walecka and P. A. Zucker, Phys. Rev. 167, 1479 (1968); P. A. Zucker, Phys. Rev. D 4, 3350 (1971).
[39]K. Holinde, K. Erkelenz, and R. Alzetta, Nucl. Phys. A194, 161 (1972).
[40]R. A. Bryan and B. L. Scott, Phys. Rev. 177, 1435 (1969).
[41]H. P. Noyes, Annu. Rev. Nucl. Sci. 22, 465 (1973).
[42]R. A. Arndt, R. H. Hackman, and L. D. Roper, Phys. Rev. C 9, 555 (1974).
[43]J. E. Brolley, Jr., J. D. Seagrave, and J. G. Beery, Phys. Rev. 135, B1119 (1964).